Proceedings of the 7th International & 28th All India Manufacturing Technology, Design and Research Conference (AIMTDR 2018)

Investigations on the Influence of Serration Parameters on Cutting Forces

P. Bari[1][0000-0001-8131-2329], P.Wahi[1][0000-0003-2106-0881] and M. Law[1*][0000-0003-2659-4188]

[1]Machine Tool Dynamics Laboratory,
Department of Mechanical Engineering
Indian Institute of Technology Kanpur, Kanpur – 208 016, India
mlaw@iitk.ac.in

Abstract. Serrated cutters, with their complex geometries, reduce cutting forces, and hence find use in the high-productivity milling of difficult-to-cut materials. Variations in serration profiles and parameters such as amplitudes, wavelengths and phase shifts influence the degree to which cutting forces can be reduced. In an effort to develop guidelines to preferentially design serrations to reduce cutting forces and improve productivity, this paper investigates the influence of serration parameters on cutting forces. A geometric force model explaining the mechanisms contributing to reducing forces is presented, and validated experimentally. Sensitivity analysis is then carried out on the validated model to understand the influence of serration parameters. It is observed that for a sinusoidal serration profile, for defined cutting conditions, the phase shift of the serrations between successive teeth contributes more to reducing forces than the serration amplitude and/or the wavelength. These results are instructive for the design of better serrated cutters.

Keywords: Serrated Cutters, Serration Parameters, Chip Thickness, Cutting Forces, Sensitivity Analysis.

1 Introduction

Manufacturing of parts made from aluminum, nickel, and titanium based alloys used in the aerospace industries, often involves 80-90% of the bulk material being removed through machining. Meeting productivity goals for such parts requires aggressive cutting conditions with high depths-of-cuts at high speeds, which, due to the difficult-to-cut nature of these materials, remains challenging. Furthermore, increased process forces due to high-depths-of-cuts may lead to process-induced unstable chatter vibrations that may damage the tool, the part, and the machine. There is a need thus for strategies that reduce forces, avoid machining instabilities, and that do not compromise productivity goals. Cutting with serrated cutters offers one such potential solution.

Serrated cutters – an example of which is shown and contrasted with a regular end mill in Fig. 1, have complex geometries that can preferentially reduce process forces. Serrations can be sinusoidal, circular, trapezoidal, or even of the half-circular type, with each of these profiles having further variations in their amplitude, wavelength and

phase shift of the serrations between successive teeth. Serrations change and reduce the local engagements of the tool with the part, and also reduce the contact length between the tool and part. These factors, combined with the complex geometries that contribute to producing a non-uniform and continuously varying chip thickness, help reduce the process forces.

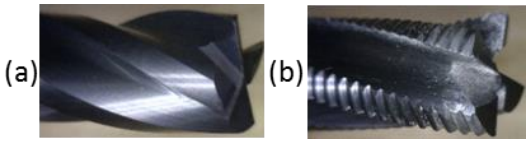

Fig. 1. (a) Regular end mill (b) Serrated end mill

Because of their ability to reduce process forces, serrated cutters have found favour in the aerospace industries. However, there appears to be no method to their designs, with all cutting tool makers preferring different profiles and serration parameters. Furthermore, even though these serrated cutters have been around for decades, focused research to make them better has not entirely informed the designs of new cutters.

Some classical early work on straight fluted serrated end mills was presented by Tlusty et al. [1], in which it was shown that due to the reduced contact between the tool and the workpiece on account of serrations, cutting forces reduce. Later, Campomanes [2] presented a detailed mechanics based model that included the influence of helix with sinusoidal serrations, and used an approximate chip thickness model [3]. Merdol and Altintas [4], and Dombovari et al. [5] reported modelling of cylindrical and tapered serrated end mills with a generalized representation of serration profiles using cubic-splines. A generalized mathematical modelling approach with arbitrary tool geometry was also proposed by Kaymakci et al. [6], wherein variation of local tool angles along serrations was included. These studies [1-6] focused more on presenting models for serrated cutters, and less on the influence of serration parameters on cutting forces. Some recent work was reported on optimizing serration profiles by Koca and Budak [7], and by Tehranizadeh and Budak [8], however they did so only for a fixed cutting parameter set.

In an effort to develop guidelines to preferentially design serrations to reduce cutting forces and improve productivity, this paper investigates the influence of serration parameters on cutting forces for two different operating conditions. We report results only for serrations of the sinusoidal kind. At first, a geometric model for serrated cutters is presented in Section 2 to help explain the mechanisms that contribute to reducing forces. Following which, the force model, explained in Section 3 is validated experimentally in Section 4. Sensitivity analysis is then carried out in Section 5 on the validated model to understand the influence of serration parameters. This is followed by the main conclusions that instruct the design of improved serrated cutters.

2 Geometric Model of Serrated Cutter

This section describes the geometry of serrated cutters that lead to a preferential reduction in cutting forces. At first, local geometries are defined, followed by describing a generalized method to model serrations, followed by regenerative delays caused by serrations. We conclude this section with discussions on variations in local chip thickness due to serrations. Models described in this section are based on the classic work done by Merdol and Altintas [4], and by Dombovari et al. [5].

2.1 Modelling of Serration Profile

A schematic, and a cross-sectional view of a sinusoidal serrated cutter is shown in Fig. 2. *xyz* coordinate frame is attached to the tool as shown. The cutter can have N number of flutes (teeth), but as an example, only three (i^{th}, $(i+1)^{th}$ and $(i+l)^{th}$) flutes are shown in Fig. 2.

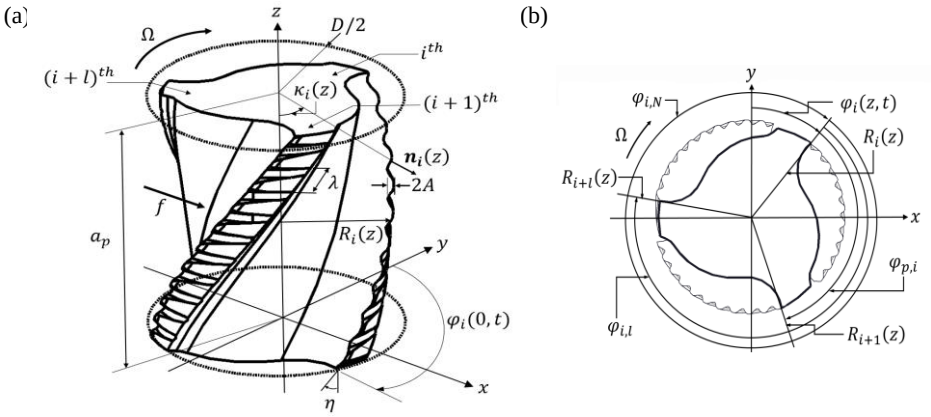

Fig. 2. (a) Geometry of the serrated cutter. (b) Cross-sectional view at height $\boldsymbol{z}$. Figure is adapted and modified from [5].

As there is a wavy surface along the flute of the serrated cutter, the local radius changes along the flute and the height. The local radius for the i^{th} flute at the height z is defined as:

$$R_i(z) = \frac{D}{2} - \Delta R_i(z), \tag{1}$$

wherein D is shank diameter of the cutter, and $\Delta R_i(z)$ is the variation in local radius for the sinusoidal serration profile:

$$\Delta R_i(z) = A - A\,sin\left(\frac{2\pi z}{\lambda \cos\eta} - \psi_i\right), \tag{2}$$

wherein A is the serration amplitude which is half of peak to peak serration height; λ is the wavelength; η is the helix angle; and ψ_i is the phase shift.

The local radius for a representative four-fluted sinusoidal serrated cutter, with parameters as measured and listed in Table 1, is shown in Fig. 3 wherein radius varies with a peak value of 8 mm for an amplitude of 0.22 mm, and a wavelength of 1.62 mm.

Table 1. Parameters of the serrated tool under consideration.

Serration profile	Serration Amplitude	Wave-length	Shank diameter	Initial phase shift	Helix angle	Rake angle	No of flutes	Cutter type
Sinusoidal	$A =$ 0.22 mm	$\lambda =$ 1.62 mm	$D = 16$ mm	ψ =[107 199 236 326] degree	η =20 degree	10 degree	$N = 4$	Cylindrical Serrated end mill

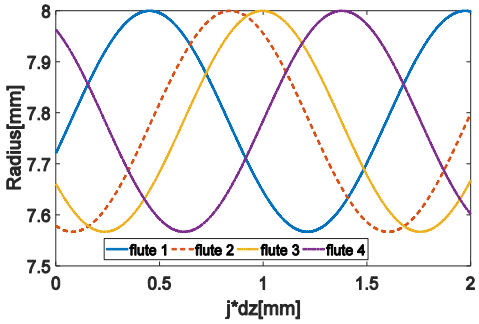

Fig. 3. Variation of local radius along height.

There is phase shift in the serration profile of each flute since the serrations start differently for different flutes. This creates a variation of local radius along the flute and height. The angular phase shift at the starting is given by:

$$\psi_i = \sum_{k=1}^{i-1} \varphi_{p,k}, \tag{3}$$

wherein $\varphi_{p,k}$is the pitch angle between the k^{th} and $(k+1)^{th}$ flute, and $\psi_1 = 0$. The angular position for the i^{th} flute at height z, measured from the y axis in a clockwise direction, called the instantaneous radial immersion angle, is calculated as follows:

$$\varphi_i(z,t) = \Omega t + \sum_{k=1}^{i-1} \varphi_{p,k} - \frac{2z \tan \eta}{D}, \tag{4}$$

wherein Ω is the clockwise spindle speed (rad/sec).

For serrated cutters, there is also an axial immersion angle that is the angle between the z axis of the cutter and the normal vector $\boldsymbol{n_i}(z)$ to the local flute tangent, as shown in the Fig. 2(a). It is expressed by the derivative of the local radius for the i^{th} flute at the height z as follows:

$$\cot \kappa_i(z) = \frac{dR_i(z)}{dz}. \tag{5}$$

As discussed above, the local radius, the instantaneous radial immersion angle, and the axial immersion angle, all vary along height of the serrated cutter, and their variation is described next, in subsection 2.2.

2.2 Variation of Tool Geometry

Since geometry changes along the height, the serrated cutter is considered to be an assembly of small differential axial disc elements, and the variation in geometry is described across each element. Local tool angles such as the rake angle ($\gamma_{n,i}(z)$), the axial immersion angle ($\kappa_i(z)$), and the helix angle ($\eta_i(z)$) are calculated in the rake face coordinate frame – shown in Fig. 4. This rake face coordinate frame is defined in each element relative to tool reference coordinate frame that is fixed at the bottom end of the tool, using a transformation as in [6]. All local angles vary due to a change in the direction of the rake face frame across each element. As a representative example, variation of axial immersion angle along the serration profile is shown in Fig. 4(c).

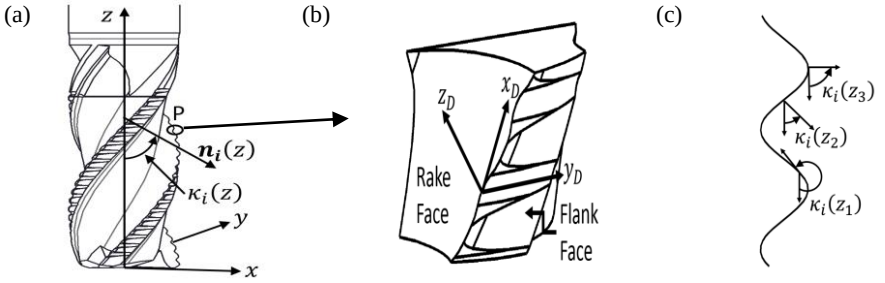

Fig. 4. (a) Schematic of complex serrated end mill (b) Rake face coordinate frame (c) Variation of axial immersion angle.

In addition to the complex variations in the local geometries, cutting with serrated cutters can also lead to missed-cut effects due to delays between the cut surfaces being generated, as discussed next in subsections 2.3. and 2.4.

2.3 Regenerative Multiple Delays between the Serrated Flutes

Due to the serration profile and changes in the local radius across the height of the cutter, it is possible that the cut surface generated previously, was made either by the same flute in the previous pass or by other flutes in same pass. This leads to multiple delays, where delay is the time elapsed between formation of the current surface being generated and the previous surface generated.

If the current cut surface is made by the i^{th} flute at time t, and the previous cut surface was made by $(i+l)^{th}$ flute at time $t-\tau_{i,l}(z)$, then at the same angular position one can rewrite the instantaneous radial immersion angle as (Ref. Fig. 2(b)):

$$\varphi_i(z,t) = \varphi_{i+l}\big(z, t-\tau_{i,l}\big), \tag{6}$$

wherein $\tau_{i,l}$, the multiple delay term in serrated cutters is:

$$\tau_{i,l} = \frac{\varphi_{i,l}}{\Omega} = \frac{1}{\Omega}\sum_{k=1}^{l-1} \varphi_{p,(i+k)\ mod\ N}. \tag{7}$$

This delay is used in the estimation of the local chip thickness as discussed next in subsection 2.4.

2.4 Local Chip Thickness

Elemental geometric static chip thickness is defined as the local distance between previous and current cut surface in the direction of normal vector $n_i(z)$ of the flute as:

$$h_{g,ie}^{st}(z,t) = \min_{l=1}^{N}[(R_i(z) - R_{i+l}(z)) + f_{i,l}(z,t)\sin\phi_i(z,t)]sin\,\kappa_i(z), \quad (8)$$

wherein $f_{i,l}(z,t)$ is the corresponding feed motion during $\tau_{i,l}$ and $R_i(z)$ is calculated from eqs. [1-2]. This however, does not signify the actual physical chip thickness. Elemental physical static chip thickness is calculated by multiplying two screening functions as:

$$h_i^{st}(z,t) = g_i(z,t)\, h_{g,ie}(z,t), \quad (9)$$

where $g_i(z,t) = g_{ri,i}(z,t)g_{h,i}(z,t)$,

wherein the screening function due to radial immersion is:

$$g_{ri,i}(z,t) = \begin{cases} 1 & \text{if } \varphi_{en} \le (\,\varphi_i(z,t)\ mod\ 2\pi) \le \varphi_{ex} \\ 0 & \text{otherwise} \end{cases} \quad (10)$$

and the screening function due to missed cut effect is:

$$g_{h,i}(z,t) = \begin{cases} 1 & \text{if } h_{g,ie}^{st}(z,t) \ge 0 \\ 0 & \text{otherwise} \end{cases}. \quad (11)$$

When the geometric chip thickness becomes negative due to the inclusion of variation of local radius in chip thickness (eq. [8]) then those corresponding flute(s) do not cut the surface. This is called the missed cut effect which causes non-uniform chip thickness, and can also be understood from Fig. 5(a).

Table 2. Operating Conditions

Case no	Depth of cut	Spindle speed	Feed rate	Radial immersion
1	2 mm	8000 rpm	0.02 mm/rev/tooth	100 % (slotting)
2	6 mm	10000 rpm	0.1 mm/rev/tooth	50% down milling

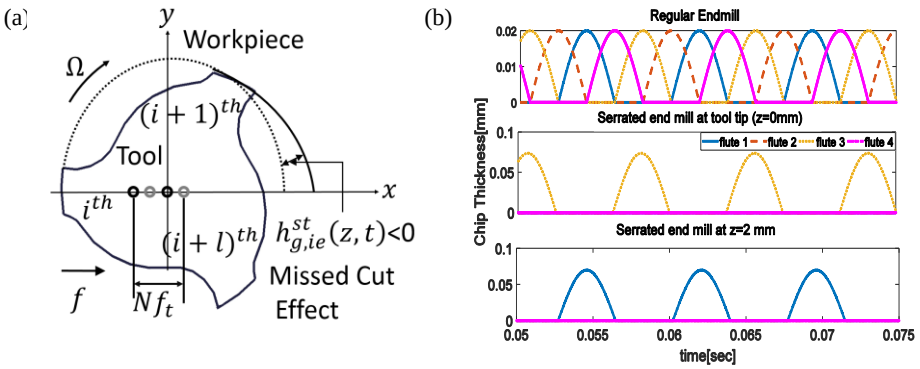

Fig. 5. (a) Possible missed-cut effect of the serrated tool. Figure is adapted and modified from [5]. (b) Chip thickness distributions for four fluted regular and serrated end mill.

Variation in the chip thickness profile for the four-fluted sinusoidal serrated cutter under consideration with cutting conditions as in Case 1, listed in Table 2, is shown in Fig. 5(b). Fig. 5(b) shows that for regular end mill all four flutes are always in cutting condition. It also shows that at the tool tip of serrated cutter only the 3rd flute is sharing the chip load and the others are in rest i.e. no cutting. But at $z = 2$ mm (from the bottom) of the serrated cutter, only the 1st flute is sharing the load. This irregular chip distribution of serrated cutters produces periodic cutting forces with non-uniform amplitudes, which contributes to a reduction in instantaneous cutting forces, as explained in Section 3.

3 Force Model for Serrated Cutter

All differential elemental forces are calculated in each element of the discretized serrated tool. The cutting forces for the i^{th} flute at a height z are found in the radial-tangential-and-axial, i.e. rta directions as shown in Fig. 6. Due to variation of the local tool geometry along the serrations, and along the axis of the tool, this rta frame changes its orientation – see Fig. 6 (b). Differential forces evaluated in the rta frame are given by:

$$d\boldsymbol{F}_{\boldsymbol{rta},i}(z,t) = [\boldsymbol{K^c} h_i^{st}(z,t) + \boldsymbol{K^e}] \frac{dz}{sin\ \kappa_i(z)} g_i(z,t), \tag{12}$$

wherein primary cutting force coefficient vector is:

$$\boldsymbol{K^c} = \boldsymbol{K^c}\big(h_i^{st}(z,t), v_{c,i}(z), \gamma_{n,i}(z)\big) = [K_r^c \quad K_t^c \quad K_a^c]^T \tag{13}$$

and the edge cutting force coefficient vector is:

$$\boldsymbol{K^e} = \boldsymbol{K^e}\big(v_{c,i}(z), \gamma_{n,i}(z)\big) = [K_r^e \quad K_t^e \quad K_a^e]^T, \tag{14}$$

wherein v is the cutting speed, and shows that in addition to being dependent on the local rake angle and the chip thickness, the coefficients also depend on the speed.

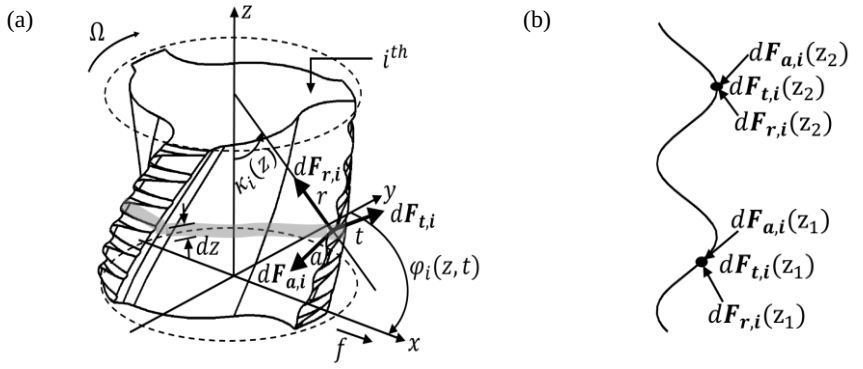

Fig. 6. (a) Differential forces acting on an infinitesimal dz *a*xial segment on the i^{th} edge. (b)Varitation of cutting force along flute and geight. Figure is modified from [5].

Differential forces evaluated in the rta frame are transformed to the fixed machine coordinate frame (xyz) using the orthogonal to oblique transformation method [9]. Transformed differential forces in the xyz frame are given by:

$$d\boldsymbol{F}_{\boldsymbol{xyz},i}(z,t) = \boldsymbol{T}_{\boldsymbol{xr},i}(z,t)d\boldsymbol{F}_{\boldsymbol{rta},i}(z,t), \tag{15}$$

wherein the force transformation matrix is given by

$$\boldsymbol{T}_{\boldsymbol{xr},i}(z,t) = \begin{bmatrix} -\sin\varphi_i \sin\kappa_i & -\cos\varphi_i & -\sin\varphi_i \cos\kappa_i \\ -\cos\varphi_i \sin\kappa_i & \sin\varphi_i & -\cos\varphi_i \cos\kappa_i \\ \cos\kappa_i & 0 & -\sin\kappa_i \end{bmatrix}, \tag{16}$$

with $\varphi_i := \varphi_i(z,t)$, $\kappa_i := \kappa_i(z)$.

The total lumped cutting force vector acting on the cutting tool in the x, y and z directions is calculated by integrating the differential force vector along flute and summing the contribution of all flutes:

$$\boldsymbol{F}_{\boldsymbol{xyz}}(t) = \begin{bmatrix} F_x & F_y & F_z \end{bmatrix}^T = \sum_{i=1}^{N} \int_0^{a_p} d\boldsymbol{F}_{\boldsymbol{xyz},i}(z,t). \tag{17}$$

Due to the serrations, only a very small portion of the flute is actually in contact with the workpiece. The apparent axial edge contact length reduces as shown in Fig. 7(a) ($a_1 + a_2 + a_3$ becomes a/N). The highlighted white portion in Fig. 7(a) is the out of cut portion (negative contact), and the shaded grey portion is the actual cutting portion (positive contact). Hence in white portions, cutting forces are zero and less than regular end mills, whereas in the grey portions, cutting forces are more than regular end mills.

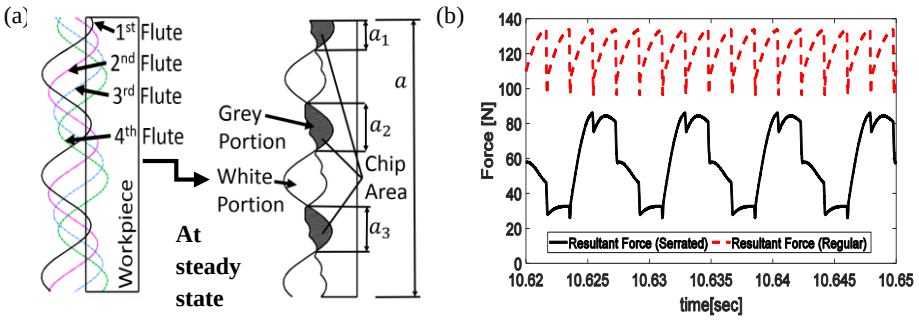

Fig. 7. (a) Schematic of apparent axial depth of cut for a four fluted serrated cutter. Figure is modified from [4]. (b) Comparison of cutting forces between serrated and regular end mill.

When the white portions dominate over grey portions, as they do with serrated cutters, overall cutting forces reduce. This reduction in forces is calculated by substituting $h_i^{st}(z,t)$ from eq. [9] into eq. [12] and finally solving eq. [17] which is demonstrated through simulation results in Fig. 7(b), which shows the resultant forces in the x-y plane for a regular end mill as well as for a serrated cutter with cutting conditions as in Case 1 – listed in Table 2. The force model presented here is validated experimentally next in Section 4.

4 Experimental Validation of Cutting Forces

The experimental setup to measure and validate the force model discussed in Section 3, is shown in Fig. 8. A three axis vertical milling machine was instrumented with a three component table top dynamometer, on which the workpiece was directly mounted. An Aluminium alloy, Al7075 was cut with cutting conditions as in Case 1 – listed in Table 2. Serrated cutter parameters are as in Table 1. Al7075 was specifically chosen, since the geometry dependent cutting force coefficients (from eq. [13] and [14]) for the corresponding tool and workpiece (Al7075) are available for this material, as given in [4, 5]. The comparison between predicted and experimental resultant cutting forces in the x-y plane is shown in Fig. 9.

Fig. 8. Experimental Setup

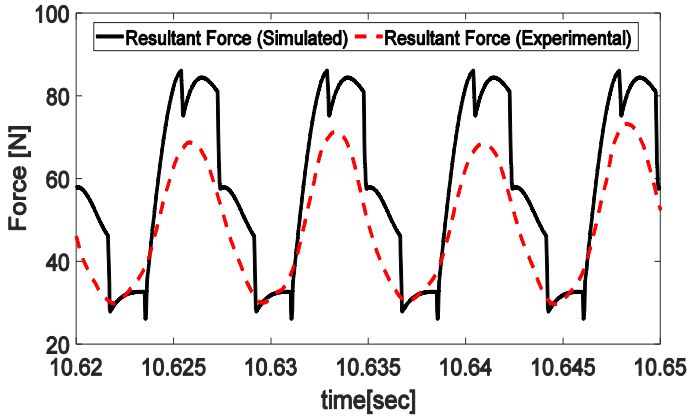

Fig. 9. Comparison of measured and predicted forces for serrated end mill.

While the mean value for measured and modelled forces match reasonably well, the measurements do not reproduce the intermittency of the modelled forces. This could potentially be attributed to the low pass filter of the control unit of dynamometer. The cut-off frequency of the built in filter within the control unit at 200 Hz is too low with respect to tooth passing frequency $\left(=\frac{8000\times4}{60}\text{Hz} = 533.3\text{ Hz}\right)$ as in Case 1 – listed in Table 2. Due to low pass filter actual signal is bypassed and local peaks are not observed in the simulated force profile. Treating the force model to be validated, sensitivity of forces to changes in serration parameters is discussed in Section 5.

5 Sensitivity of Cutting Forces to Changes in Serration Parameters

Sensitivity analysis is carried out by increasing (doubling) and decreasing (halving) the serration amplitude and the wavelength, in turn, while keeping all other parameters fixed. Sensitivity to changes in the phase shift are also discussed. All analysis is done for two sets of cutting conditions as listed in Table 2. For all results, model predicted resultant forces in the x-y plane for the original serration parameters are compared with forces obtained with a change in parameters.

5.1 Influence of a Change in Serration Amplitude

Keeping other parameters fixed, amplitude of the serrations are changed (increased and decreased) to investigate its influence on the predicted resultant cutting force shown in Fig. 10. For cutting with parameters of Case 1 (Fig. 10(a)), it is observed that the maximum resultant force corresponding to original amplitude (0.22 mm), double amplitude (0.44 mm) and half amplitude (0.11 mm) are ~87 N, ~90 N (~4% increase) and ~88N (~1.3% increase). For Case 2 (Fig. 10(b)), corresponding forces are ~662 N, ~677 N (2.3 % increase) and ~617 N (~7% decrease).

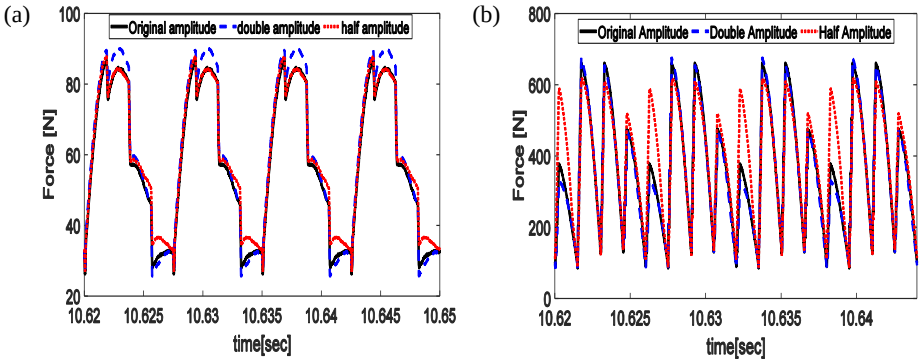

Fig. 10. Influence of a change in amplitude of serrations on resultant force (a) Case 1 (b) Case 2

As is clearly evident, the resultant force does not appear to be very sensitive to a change in the serration amplitude, for cutting with either of the cutting parameter set.

5.2 Influence of a Change in Serration Wavelength

Influence of a change in serration wavelength as compared to the original wavelength can be understood by the comparisons of the predicted resultant cutting forces in Fig. 11. For Case 1 it is observed that the maximum resultant force corresponding to original wavelength (1.62 mm), double wavelength (3.24 mm) and half wavelength (0.81 mm) are ~87 N, ~106 N (~22 % increase) and ~85 N (~2% decrease). For Case 2 corresponding forces are ~661N, ~658 N (no appreciable change) and ~681N (~3 % increase). It

may hence be concluded that for specific combinations of cutting parameters, doubling of the serration wavelength, may adversely increase the cutting forces, pointing to the fact that wavelength might be an important parameter while designing serrated cutters.

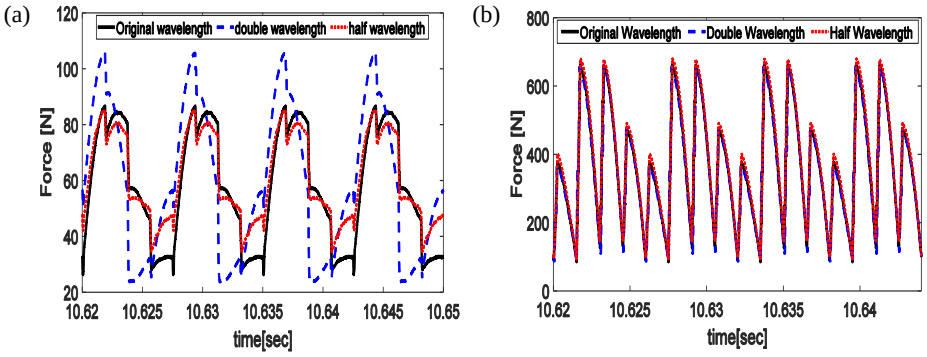

Fig. 11. Influence of a change in wavelength on resultant force (a) Case 1 (b) Case 2

5.3 Influence of a Change in Serration Phase Shift

Influence of a change in serration phase shift as compared to the original phase shift can be understood by the comparisons of the predicted resultant cutting forces in Fig. 12.

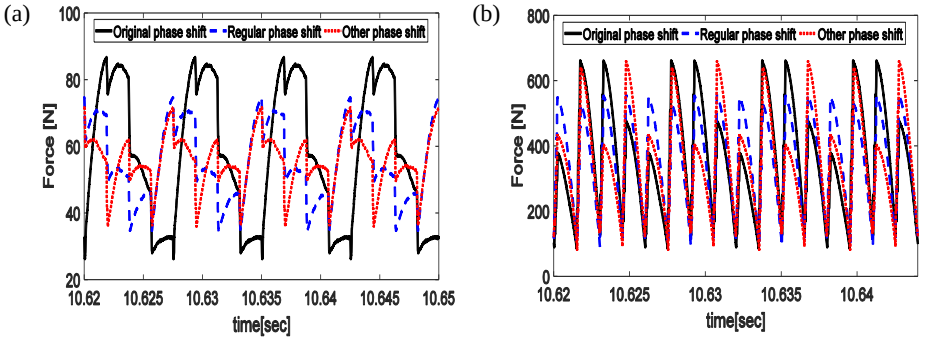

Fig. 12. Influence of a change in phase shift on resultant force (a) Case 1 (b) Case 2

For cutting with the parameters of Case 1 (Table 2) it is observed that the maximum resultant force corresponding to the original phase shift ([107 199 236 326] degree), regular phase shift ([0 90 180 270] degree) and other phase shift ([270 90 180 0] degree) are ~87 N, ~75 N (~14 % decrease) and ~72 N (~17 % decrease). For Case 2, corresponding forces are ~661 N, ~557 N (~16 % decrease) and ~661 N (~0.1 % decrease). From this analysis it may be concluded that for specific combinations of cutting parameters, a change in phase shift can preferentially reduce cutting forces. From the sensitivity analysis, it is evident that forces appear to be consistently more sensitive to a change in phase shift as compared to a change in serration amplitude and/or wavelength

– thus suggesting that phase shift is also an important factor to be considered while designing serrated cutters that could potentially result in improved reduction of cutting forces.

6 Conclusions

This paper discussed the influence of serration parameters on cutting forces. For a serrated cutter with a sinusoidal serration pattern, an experimentally validated force model was subject to sensitivity analysis to explore the role of serration amplitude, wavelength, and the phase shift of the serrations between successive teeth. Sensitivity analysis was carried out with two different sets of cutting conditions. For the cases investigated, the amplitude of the serration was found to be an insignificant design parameter as we get maximum ~7% decrease in resultant force. It was also observed that the phase shift and the serration wavelength can significantly influence cutting forces, with forces either increasing (maximum ~22% increase due to wavelength) or reducing (maximum ~17 % decrease due to phase shift) depending on the combination of cutting and serration parameters. These results clearly motivate the need for a well-designed optimization study that will include the influence of different types of serration profiles and their parameters for a wide range of cutting conditions – which forms part of the planned future work, with the ultimate aim of this study being to inform the design of next-generation of serrated cutters that preferentially reduce cutting forces.

References

1. J. Tlusty et al., “Use of Special Milling Cutters against Chatter,” Proceeings of *NAMRC 11*, SME, 1983.
2. M. L. Campomanes, “Kinematics and dynamics of milling with roughing tools,” *Metal Cutting and High Speed Machining*, 2002.
3. Y. Altintas and A. Ber, *Manufacturing Automation: Metal Cutting Mechanics, Machine Tool Vibrations, and CNC Design*, 2001.
4. S. D. Merdol and Y. Altintas, “Mechanics and Dynamics of Serrated Cylindrical and Tapered End Mills,” *J. Manuf. Sci. Eng.*, 2004.
5. Z. Dombovari et al., “The effect of serration on mechanics and stability of milling cutters,” *Int. J. Mach. Tools Manuf.*, 2010.
6. M. Kaymakci et al., “Unified cutting force model for turning, boring, drilling and milling operations,” *Int. J. Mach. Tools Manuf*, 2012.
7. R. Koca and E. Budak, “Optimization of serrated end mills for reduced cutting energy and higher stability,” *Procedia CIRP*, 2013.
8. F. Tehranizadeh and E. Budak, “Design of Serrated End Mills for Improved Productivity,” *Procedia CIRP*, 2017.
9. E. Budak et al., “Prediction of Milling Force Coefficients From Orthogonal Cutting Data,” *J. Manuf. Sci. Eng.*, 1996.